Journal of Applied Physics ARTICLE pubs.aip.org/aip/jap

Analytical models for the thermal properties of n-type porous silicon layers: Dependence of porosity

Cite as: J. Appl. Phys. **137**, 085103 (2025); doi: 10.1063/5.0250168
Submitted: 22 November 2024 · Accepted: 31 January 2025 ·
Published Online: 26 February 2025

Joel Hernández-Wong,[1] Uriel Nogal Luis,[1] Alejandro Rojas Marroquin,[1] Lizbeth Luviano Elizalde,[2] José Bruno Rojas-Trigos,[3] Ernesto Marin Moares,[3] and Antonio Calderon[3,a)]

AFFILIATIONS

[1]Centro de Investigación en Ciencia Aplicada y Tecnología Avanzada, CONAHCyT-Instituto Politécnico Nacional, Legaria 694, Col. Irrigación, 11500 Ciudad de México, Mexico
[2]Departamento de Ciencias Básicas, Universidad Tecnológica Fidel Velázquez, Av. Emiliano Zapata S/N, Col. El tráfico, C.P. 54474 Nicolás Romero, Estado de México, Mexico
[3]Centro de Investigación en Ciencia Aplicada y Tecnología Avanzada, Instituto Politécnico Nacional, Legaria 694 Col. Irrigación, 11500 Ciudad de México, Mexico

[a)]**Author to whom correspondence should be addressed:** jcalderona@ipn.mx

ABSTRACT

Several reports in the literature concern the thermal properties of porous silicon samples considering the porous layer plus the silicon substrate, but not so of the porous layer in particular. This work uses the frequency domain photoacoustic technique in a heat transmission configuration together with an analysis based on a composite two-layer model of thermal resistances on *n*-type porous silicon and the porosity concept to develop a non-separative (and hence non-destructive) methodology for determining the thermal properties of the porous layer of *n*-type porous silicon and provide analytical models to obtain such properties as a function of its porosity. The porous silicon samples were elaborated by anodization, with anodization times from 10 to 100 min on (100)-oriented *n*-type crystalline silicon wafers and using a 48% hydrofluoric acid water solution. These wafers were non-degenerated, phosphorous doped, 500 μm roughly thick, and had 1.72 Ω cm electrical resistivity. In each sample, gravimetry determined porosity ranging from 0.279 to 0.702, and the porous layer's thickness was determined by electron microscopy. An analytical expression was obtained for the effective thermal diffusivity of the n-type porous silicon as a whole. After fitting it to the data obtained by the photoacoustic measurements, a value around 0.076 cm^2/s, independent of porosity, was obtained for the thermal diffusivity of the porous layer. In addition, analytical expressions were obtained for the porous layer's thermal conductivity, volumetric heat capacity, and thermal effusivity, all showed a decreasing linear dependence on the porosity.

I. INTRODUCTION

Porous silicon (PSi) consists essentially of a layer with a porous structure on top of a substrate of crystalline silicon (CSi). Several methods have been developed to elaborate PSi from CSi.[1] Anodization is the most extensively used so far, mainly because it allows precise control of the thickness and porosity of the porous structure, allowing the fabrication of large-area PSi samples.[2–4] This method anodically polarizes the CSi wafer in a hydrofluoric (HF) acid electrolytic solution. Pore generation on the surface of a CSi wafer is known as anodization, and the porosified layer is called the porous layer. The porous structure obtained in *p*-type CSi wafers is sponge-like, while for *n*-type CSi wafers, it is a columnar arrangement.[5,6] Since its discovery in the middle of the past century,[7] interest in PSi has grown significantly, and its applications have extended to various fields, from electronics to biomedicine.[8–11] These applications require studying and knowing the materials physical properties, of which thermal properties are essential in many cases. This work is focused on the thermal characterization of *n*-type PSi, for which literature reports are scarce compared with those on *p*-type material. In reported works, the thermal properties of PSi as a whole (porous layer plus CSi substrate) are reported, but not those of the porous layer.[12–16] This is understandable because

separating the porous layer from the substrate can be very complicated, being able to destroy the sample. This work aims to develop a methodology for determining the thermal properties of n-type porous silicon's porous layer by obtaining analytical models of such properties as a function of its porosity.

II. ANALYTICAL RESULTS

A. Two-layer model for the *n*-type porous silicon structure

An electrochemically formed *n*-type PSi is a two-layer system of total thickness l, consisting of a porous layer (labeled with number 1) with thickness l_1, on top of a silicon substrate (labeled with number 2) with thickness l_2. Figure 1 shows an SEM side view of a PSi sample elaborated with 60 min of anodization time and the corresponding schematic representation. Figure 1(a) shows the columnar structure of the porous layer. Figure 1(b) shows the schematic representation of the PSi sample as a two-layer system.

At the beginning of the anodizing process, the electrochemical reaction erodes the substrate surface and forms tiny pores (voids) that become deeper with the anodization time, increasing the thickness of the porous layer. The electrochemical reaction also occurs on the walls of the voids, widening them until they merge and form columns of solid material. The chemical reaction continues to thin the columns, increasing the PSi samples' porosity. Figure 2 shows a close-up of the side view of the porous layer of the PSi sample elaborated with 30 min of anodization time. The diameters of the columns of solid material are smaller in areas close to the surface than in deeper areas due to the longer exposure time to the electrochemical reaction.

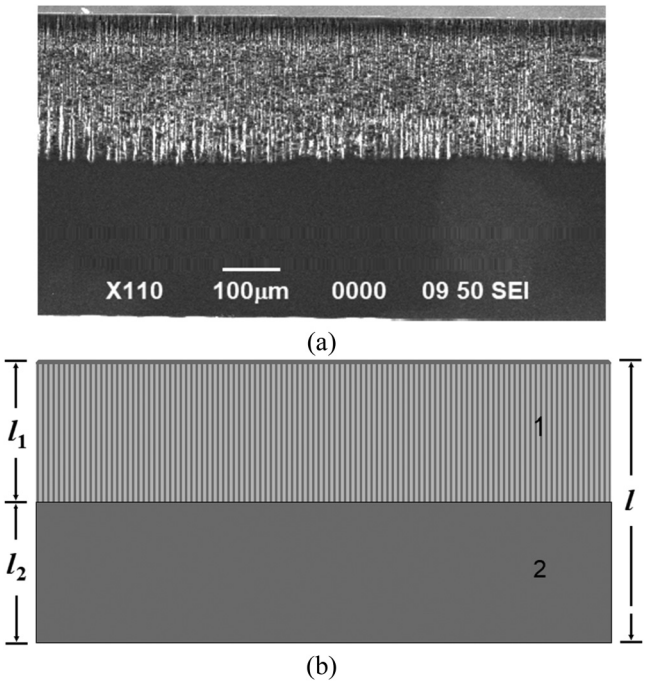

FIG. 1. (a) SEM side view of a PSi sample elaborated with 60 min of anodization time. (b) Schematic representation of PSi sample. Number 1 denotes the porous layer, and number 2 the silicon substrate.

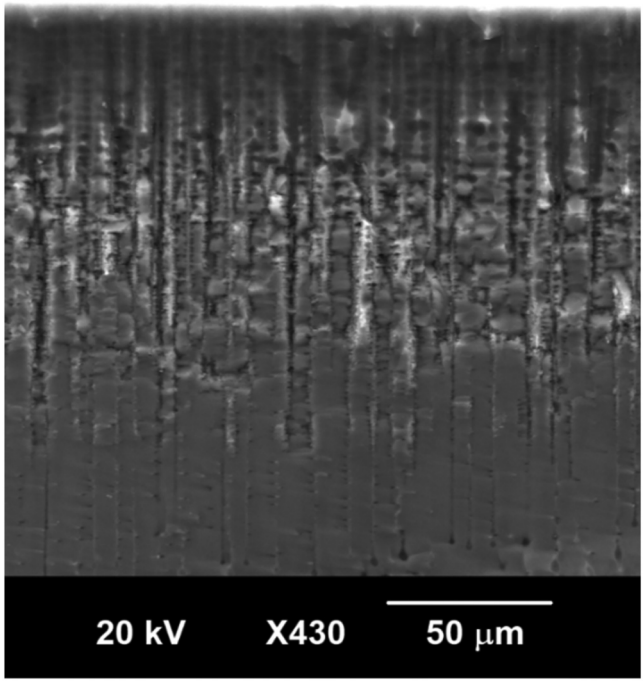

FIG. 2. SEM side view of the porous layer of the PSi sample elaborated with 30 min of anodization time.

In the side view of the PSi samples, a thin surface layer (mainly consisting of silicon oxides) can be distinguished over the macroporous layer. The front view of this layer for the PSi samples elaborated with 30 and 60 min are shown in Figs. 3(a) and 3(b), respectively. A porous surface is observed in both images. In Fig. 3(a), approximately circular voids with diameters less than 1 μm are observed, while in Fig. 3(b) the voids are wider, and many have a cross shape due to the collapse between neighboring voids. This surface layer hides the surface porous structure of the macroporous layer, so it is not observed in the images in Fig. 3.

B. Porosity of the porous silicon layer

If m_{s_i} and m_{s_f} represent the masses of the complete sample before and after the anodization, respectively, then the mass Δm of the CSi material removed by the anodic dissolution can be written as

$$\Delta m = m_{s_i} - m_{s_f}. \tag{1}$$

The porous layer's porosity $p(0 < p < 1)$ is defined as the volume fraction that the air occupies in this layer,

$$p = \frac{V_a}{V_1}, \tag{2}$$

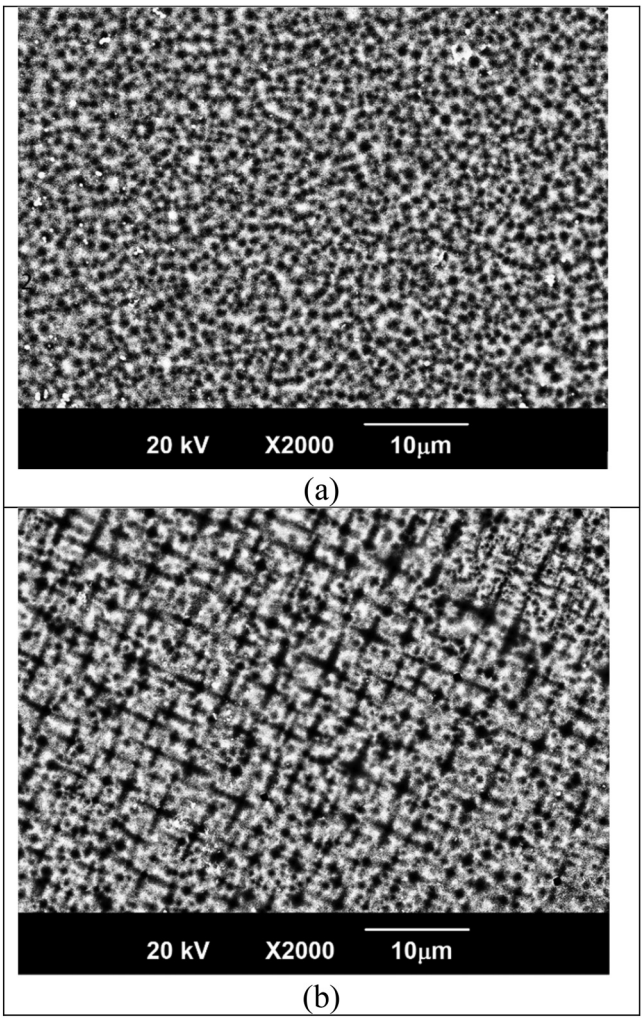

FIG. 3. SEM front view of the porous layer of the PSi samples elaborated with (a) 30 and (b) 60 min of anodization time.

with V_a being the volume occupied by the air in the porous layer of volume V_1. Since the density of CSi removed is $\rho_{Si} = \Delta m/V_a$, then

$$p = \frac{(\Delta m/\rho_{Si})}{V_1}. \tag{3}$$

Denoting by m_{1_i} the mass of layer 1 before the anodization process, we have $\rho_{si} = m_{1i}/V_1$. Then, if m_{1_f} is the mass of layer 1 after the anodization process and m_2 is the mass of layer 2 or CSi substrate, Eq. (3) can be rewritten as

$$p = \frac{\Delta m}{m_{1_i}} = \frac{m_{s_i} - m_{s_f}}{m_{s_i} - m_2}. \tag{4}$$

Thus, the porosity p of the porous layer can be determined from Eq. (4) if the masses involved in it are well known. Yon *et al.* reported an accuracy of up to 2% of Eq. (4).[17]

C. Heat capacity of the porous silicon layer: Dependence on porosity

The heat capacity is an extensive property, so the heat capacity of the porous layer can be written as

$$V_1\rho_1 c_1 = V_a\rho_a c_a + V_{mc}\rho_{mc}c_{mc}, \tag{5}$$

where ρ is the density, c is the specific heat, and the sub-indexes a and mc denote the air and the material of the columns in the porous layer, respectively. Then, using Eqs. (2) and (5), the porous layer volumetric heat capacity can be written as

$$\rho_1 c_1 = p \cdot \rho_a c_a + (1-p) \cdot \rho_{mc} c_{mc}. \tag{6}$$

Note that $V_{mc} = V_1 - V_a$.

Taking into consideration that the solid material in the porous layer is essentially composed of CSi and silicon oxides, mainly SiO_2,[2,3] that $\rho_{si}c_{si} = 1.66\ \text{J cm}^{-3}\ \text{K}^{-1}$, $\rho_{SiO_2}c_{SiO_2} = 1.705 - 2.31\ \text{J cm}^{-3}\ \text{K}^{-1}$, and $\rho_{air}c_{air} = 1.17\ \text{J cm}^{-3}\ \text{K}^{-1}$,[18,19] Eq. (6) can be reduced to

$$\rho_1 c_1 \approx (1-p) \cdot \rho_c c_c, \tag{7}$$

where ρ_c and c_c are the density and specific heat of columns, respectively, it was considered that $\rho_{mc} = \rho_c$ and $c_{mc} = c_c$ because ρ and c are intensive properties. This result means that the increase in porosity p leads to a decrease in the volume fraction occupied by the solid material in the porous silicon layer, $1-p$, and hence a decrease in its volumetric heat capacity has a linear porosity dependence.

D. Thermal conductivity of the porous silicon layer: Dependence on porosity

Considering the porous layer of n-type PSi as an array of air-embedded free-standing parallel columns, this layer can be treated as an array of parallel thermal resistances to the heat flow in the heat transmission configuration of the photoacoustic (PA) technique (see later). Because the thermal conductivity of the air is several orders of magnitude lower than the columnar material compound of silicon and silicon oxides ($k_{air} = 2.6 \times 10^{-4}\ \text{W cm}^{-1}\ \text{K}^{-1}$,[20] $k_{si} = 1.48\ \text{W cm}^{-1}\ \text{K}^{-1}$, $k_{SiO_2} = 1.1 - 1.5 \times 10^{-2}\ \text{W cm}^{-1}\ \text{K}^{-1}$),[21] then, with a good approximation, we can consider the equivalent thermal resistance of the porous layer, R_1, equal to the equivalent thermal resistance of the array of solid material columns, R_{mx},

$$R_1^{-1} = R_{mc}^{-1} = \sum_i \frac{1}{R_{c_i}}, \tag{8}$$

where summation is carried out for all columns in the porous layer and R_{ci} is the thermal resistance of the ith column. Considering that A_{ci} and K_{ci} are the cross-sectional area and the thermal conductivity of the ith column, respectively, then from Fourier's law for heat conduction, $R_{ci} = l_1/A_{ci}k_{ci} = l_1^2/V_{ci}k_{ci}$, where $V_{ci} = l_1 A_{ci}$ is the volume

of the ith column. Replacing this result, and $R_1 = l_1/A_1k_1 = l_1^2/V_1k_1$, in Eq. (8), and reducing, it follows

$$V_1k_1 = k_c\sum_i V_{c_i}, \tag{9}$$

where $k_{mc} = k_{ci}$ because thermal conductivity is an intensive physical property, and for the same reason, $k_{ci} = k_c$, with k_c being the thermal conductivity of columns. Remembering that $V_{mc} = V_1 - V_a$, and using Eq. (2), Eq. (9) reduces to

$$k_1 = (1-p)k_c. \tag{10}$$

This equation is similar to Eq. (7). The thermal conductivity of the porous layer shows a linear decrease with the porosity and direct proportional dependence to the columnar material's thermal conductivity.

E. Thermal diffusivity of the porous silicon layer

The thermal diffusivity of the porous silicon layer is related to its volumetric heat capacity and its thermal conductivity as[22]

$$\alpha_1 = \frac{k_1}{\rho_1 c_1}. \tag{11}$$

Consequently, by Eqs. (7) and (10), the last equation reduces to

$$\alpha_1 \approx \alpha_c. \tag{12}$$

Therefore, the thermal diffusivity of the porous layer is practically the same for all samples, regardless of their thickness and porosity, and it should be similar to that of the columnar material. In n-type PSi, heat flows preferably through the columns of the solid phase because the thermal resistance of air is several orders of magnitude higher than that of CSi and silicon oxides.

F. Analytical models to determine porous layer thermal properties from PA measurements

By the consideration of each PSi sample as a two-layer system, the inverse of the effective thermal diffusivity, α, of the complete PSi sample for the flow perpendicular to the sample surface may be written as[23]

$$\alpha^{-1} = x^2\alpha_1^{-1} + (1-x)^2\alpha_2^{-1} + x(1-x)\left[\lambda_{12}\alpha_1^{-1} + \lambda_{12}^{-1}\alpha_2^{-1}\right]. \tag{13}$$

Here, $x = l_1/l$ is the porous layer thickness fraction and $\lambda_{12} = k_1/k_2$ is the reason between the thermal conductivity of the porous layer and that of the substrate layer.

Taking into account that the columnar material of the porous layer is made up mainly of Si and in less proportion to SiO_2[2,3] and that the volumetric heat capacity of both compounds is similar, we can consider with a good approximation that

$$(\rho c)_c \approx (\rho c)_2. \tag{14}$$

With this last consideration and Eqs. (7), (10), and (12), Eq. (13) can be reduced to

$$\alpha^{-1} = (1-xp)\left[x(1-p)^{-1}\alpha_1^{-1} + (1-x)\alpha_2^{-1}\right]. \tag{15}$$

The thermal diffusivity of the Si substrate, α_2, is a constant independent of the anodization time or porous layer thickness fraction, the same as the thermal diffusivity of the porous layer, α_1, according to the result of Eq. (12). Thus, knowing the porosity as a function of the porous layer thickness fraction, $p(x)$, the thermal diffusivity of the porous layer α_1 can be obtained from the fitting of Eq. (15) to the experimental values of α vs x.

Once the value of α_1 has been determined, the remaining thermal parameters can be obtained using Eq. (14) and the porosity value, $p(x)$. From Eq. (7), the volumetric heat capacity of the porous layer takes the form

$$\rho_1 c_1 \approx (1-p)\cdot\rho_2 c_2. \tag{16}$$

Replacing $k_c = \alpha_c\rho_c c_c$ in Eq. (10) and considering Eqs. (12) and (14), the thermal conductivity of the PSi layer takes the form

$$k_1 \approx (1-p)\alpha_1\cdot\rho_2 c_2. \tag{17}$$

Finally, from Eqs. (16) and (17), the thermal effusivity of the porous silicon layer, $e_1 = \sqrt{k_1(\rho c)_1}$, can be written as

$$e_1 = (1-p)\sqrt{\alpha_1}\cdot\rho_2 c_2. \tag{18}$$

In this form, from Eqs. (15–18), it can be obtaining the complete set of thermal parameters of the porous layer, as a function of its porosity for n-type PSi samples.

III. MATERIALS AND METHODS

The PSi samples were elaborated by anodization on (100)-oriented n-type CSi wafers non-degenerated, phosphorous doped, with 500 μm roughly thickness and 1.72 Ω cm electrical resistivity. The anodizing procedure, or electrochemical etching, is described in detail in Ref. 4. We use an anodization Teflon cell with a 2×3 cm^2 internal base and a 3 cm height. The CSi sample is placed, covering a 1 cm diameter circular hole located in one of the lateral cell's walls so that only one sample face is exposed to 48% hydrofluoric (HF) acid water solution poured into the cell. Before the anodization process, the sample was subjected to a cleaning procedure, and a silver layer was deposited on its other face, with a platinum wire fixed to it using silver paint as a connection pole to the electrical circuit. A square-shaped platinum slab with an area of 3×3 cm^2 immersed in the HF solution, aligned, parallel, and 1.5 cm away from the face of the sample was used as a cathode to ensure uniformity of the electric field established between both surfaces when energizing the circuit. For this, a 40 mA/cm^2 current density was applied by a DC power supply (Keithley-model 2400) operating 5–10 V range. During the anodization procedure, the sample surface exposed to the HF solution was kept under lighting by a 250 W infrared lamp 30 cm away from it. By considering anodization times from 10 to 100 min, we obtain PSi samples with different porous layer thicknesses.

The frequency domain photoacoustic technique in a heat transmission configuration was used to obtain the effective thermal diffusivity of the porous silicon samples at room temperature. In this technique, outlined in Ref. 24, the sample is mounted directly on the entrance of an electret microphone adhered to with vacuum grease. A laser beam of 20 mW is intensity modulated by a TTL (Transistor-Transistor-Logic) signal sent by the lock-in amplifier (SR-850) and then directed perpendicularly on the sample. The light absorbed by the surface of the sample is transformed into heat that spreads toward the other side of the sample, which is in contact with the air in the electret chamber. The heat diffuses toward the air in the chamber, generating pressure variations that are transformed into an electrical signal. The microphone output signal is received by a lock-in amplifier (SR-850) synchronized at the modulation frequency and then sent to a computer for capture. The data acquisition is automatically controlled by a computer and a GPIB (general-purpose interface bus) electronic card.

IV. RESULTS AND DISCUSSION

PSi samples were elaborated by anodization with 10, 20, 30, 40, 50, 60, 70, 80, 90, and 100 min anodization times. In each case, the thickness of the porous layer, l_1, was determined from the average of ten measurements of the lateral images obtained by scanning electron microscopy. The porous layer porosity, p, was determined using Eq. (4). Table SM-I in the supplementary material summarizes these results, together with the total thickness of each sample, l, and the porous layer thickness fraction $x = l_1/l$. Figure 4 shows the graph of porosity as a function of the porous layer thickness fraction of the PSi samples.

The solid curve shows the result of the best least squares fit using the equation

$$p(x) = a + mx, \tag{19}$$

leaving a and m as adjustable parameters. The result was $a = 0.0729 \pm 0.0196$ and $m = 1.065\,01 \pm 0.043\,71$, with a determination coefficient R^2 equal to 0.9867.

The PA response as a function of the modulation frequency was obtained from each sample using the frequency domain photoacoustic technique at room temperature and in a heat transmission configuration in a 90–240 Hz frequency range. Figure 5 shows the graph of the PA signal phase experimental data vs modulation frequency for the PSi samples described in Table SM-I in the supplementary material.

To analyze the experimental data, the following equation was used that describes the PA signal phase as a function of modulation frequency f:[25]

$$\Delta\varphi = -a\tan\left(\frac{\tan\left(\sqrt{f/f_c}\right)}{\tanh\left(\sqrt{f/f_c}\right)}\right) - \varphi_o, \tag{20}$$

where φ_o is a phase constant and

$$f_c = \frac{\alpha}{\pi l^2} \tag{21}$$

is the modulation frequency at which the thermal diffusion length $\mu = (\pi f/\alpha)^{1/2}$ matches the sample thickness, known as the characteristic frequency. The solid lines in Fig. 3 correspond to the best fits of Eq. (20) to the experimental data, leaving f_c and φ_o as adjustable parameters. The results are reported in Table SM-II in the supplementary material, which includes each sample's effective thermal diffusivity values obtained by using Eq. (21).

Figure 6 shows the graph of the effective thermal diffusivity of the PSi samples as a function of the porous layer thickness fraction. The solid line is the result of the best least squares fit of the data using Eq. (15), leaving the thermal diffusivity of the PSi layer, α_1, as the adjustable parameter and taking the substrate thermal

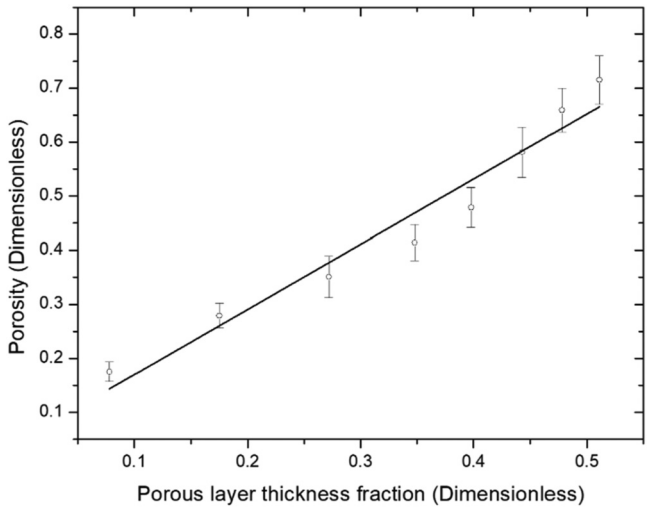

FIG. 4. PSi samples porosity vs porous layer thickness fraction.

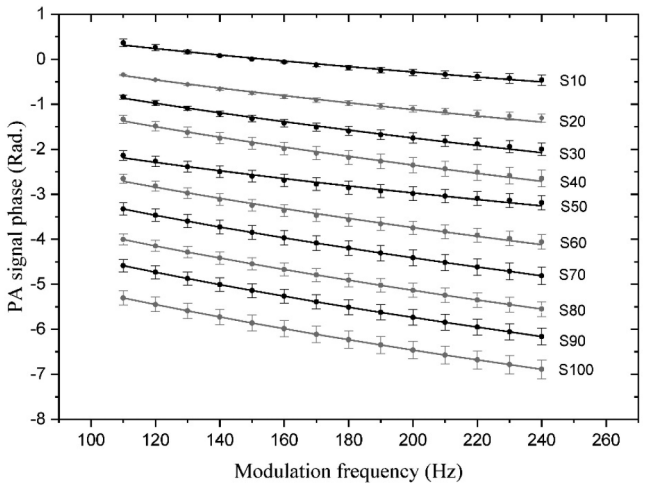

FIG. 5. Photoacoustic signal phase vs modulation frequency of the PSi samples.

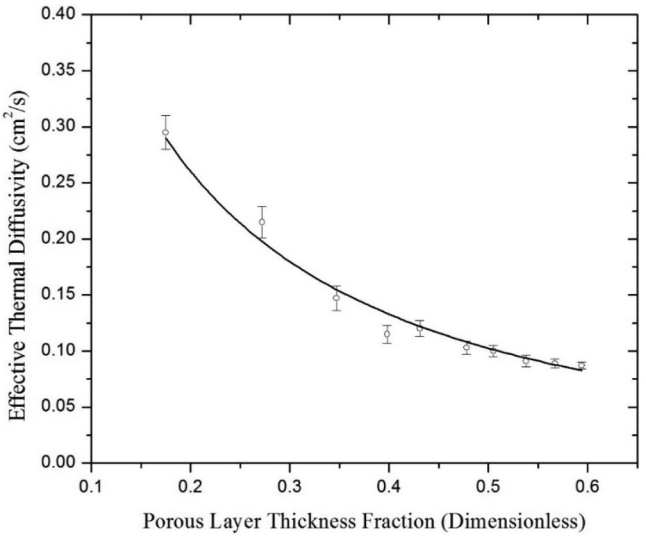

FIG. 6. Effective thermal diffusivity of the PSi samples vs porous layer thickness fraction.

diffusivity (CSi), α_2, equal to 0.88 cm^2/s, and the porosity dependence with the porous layer thickness fraction, $p(x)$, as given by Eq. (19). The result was

$$\alpha_1 = 0.076 \pm 0.002 \text{ cm}^2/\text{s}, \tag{22}$$

with a determination coefficient R^2 equal to 0.981 06.

Using the result (22) and the value of the volumetric heat capacity of the crystalline Si, $\rho_2 c_2 = 1.66$ J/cm^{3}K, in Eqs. (16–(18) the following expressions were obtained for the volumetric heat capacity, the thermal conductivity, and the thermal effusivity of the porous layers of n-type PSi as a function of porosity:

$$\rho_1 c_1 = (1 - p) \times 1.66 \text{ J/cm}^3 \text{ K}, \tag{23}$$

$$k_1 = (1 - p) \times 0.126 \text{ W/cm K}, \tag{24}$$

$$e_1 = (1 - p) \times 0.458 \text{ W s}^{1/2}\text{cm}^{-2} \text{ K}^{-1}. \tag{25}$$

It is essential to remember that these results were obtained in the 0.279–0.702 porosity range, corresponding to the 10–100 min anodization times of the studied samples.

There are no reports in the literature on the thermal properties of the porous layer in n-type PSi that we can compare with our results. However, for p-type PSi samples, Wolf and Brendel report[26] the separation of the porous layers from the Si substrate of seven samples with porosities ranging from 0.275 to 0.662 using the lock-in thermography method to determine their thermal properties. In Table I, we compare the results obtained by Wolf and Brendel with the corresponding values obtained with our models [Eqs. (22)–(24)]. Even though Wolf and Brendel analyzed p-type PSi and we used n-type PSi, the comparison of the values of the different thermal parameters agrees acceptably well for all the porosities. A significant difference in this comparison is that while the thermal diffusivity value of the porous layer for p-type PSi reduces with porosity, it remains unchanged for n-type PSi. This can be explained by the difference in porous structure between p-type and n-type PSi. The sponge-like porous structure of p-type PSi restricts the mean free path of phonons, reducing heat flow with increasing porosity and thickness of the porous layer. In the case of n-type PSi, the porous structure is columnar type. As the anodizing time increases, the erosion on the column walls increases, decreasing the amount of solid material in them and increasing the porosity (p) of the porous layer. This reduces the area for heat flow through the columnar structure, increasing the thermal resistance of the porous layer and, therefore, decreasing its thermal conductivity, see Eq. (10). Furthermore, decreased solid material in the columns due to increased porosity decreases the volumetric heat capacity, see Eq. (7). The thermal diffusivity is the reason between the thermal conductivity and the volumetric heat capacity, Eq. (11); therefore, from Eqs. (7) and (10) follow that the thermal diffusivity of the porous layer results approximately constant, Eq. (12). In general, thermal diffusivity is related to the rate at which heat propagates and its damping in the medium. A decrease in thermal conductivity reduces thermal diffusivity, and a reduction in volumetric heat capacity increases thermal diffusivity. In n-type PSi samples, the linear decrease in k and pc with porosity is compensated by each other in the porous layer, keeping its thermal diffusivity practically constant.

TABLE I. Comparison between the thermal properties values of the porous layers of PSi samples reported in Ref. 26 with our results.

	Ref. 26			Eqs. (22)–(24)		
Porosity	α (mm^2/s)	k (W/m K)	ρC (J/cm^3 K)	α_1 (mm^2/s)	k_1 (W/m K)	$(\rho c)_1$ (J/cm^3 K)
27.5 ± 0.6	14.3 ± 1.2	20.8 ± 4.6	1.46 ± 0.30	7.60 ± 0.2	9.14 ± 0.5	1.20 ± 0.04
37.2 ± 0.2	13.9 ± 1.0	12.7 ± 2.0	0.91 ± 0.13	7.60 ± 0.2	7.91 ± 0.4	1.04 ± 0.03
44.2 ± 0.2	12.5 ± 0.7	11.3 ± 2.2	0.90 ± 0.17	7.60 ± 0.2	7.03 ± 0.4	0.93 ± 0.03
48.4 ± 0.2	9.1 ± 1.3	8.7 ± 2.4	0.96 ± 0.23	7.60 ± 0.2	6.50 ± 0.4	0.86 ± 0.03
51.7 ± 0.2	9.0 ± 1.1	6.1 ± 1.2	0.68 ± 0.12	7.60 ± 0.2	6.09 ± 0.3	0.80 ± 0.02
58.8 ± 0.2	6.8 ± 0.4	4.5 ± 0.7	0.67 ± 0.09	7.60 ± 0.2	5.19 ± 0.3	0.68 ± 0.02
66.2 ± 0.2	5.1 ± 0.4	2.3 ± 0.5	0.45 ± 0.09	7.60 ± 0.2	4.26 ± 0.2	0.56 ± 0.02

To determine the thermal properties of the porous layer of n-type PSi samples, we tried to separate it from the substrate following the procedure reported in the literature.[27] In the cases where we achieved a separation, it was not complete and helpful for our photoacoustic measurements. Apparently, due to the difference in the porous structure, it is more difficult to completely separate the porous layer from an n-type PSi sample than from a p-type one. This is why we decided to develop a method that did not require realizing such separation, which led to this work.

The reports on the effective thermal properties of n-type PSi are very scarce in the literature. However, we can compare our results with the effective values of thermal effusivity and diffusivity of n-type PSi given in two references.[16,28] Gutiérrez *et al.*[28] report effective thermal effusivity (e_{eff}) values of n-type PSi and do so for porosities of 0.104 and below. To compare with our results, we determined the e_{eff} of our sample of 0.279 porosity (which has the porosity closest to that of samples of Gutiérrez *et al.*) using the photoacoustic technique and the model of Rosencwaig and Gersho[29] for a thermally thick regime, obtaining a value of 0.839 ± 0.025 W s$^{1/2}$/cm^2 K which is not very different from 1.23 W s$^{1/2}$/cm^2 K reported by Gutiérrez *et al.* Furthermore, if we consider that the e_{eff} decreases with increasing porosity, as shown by Gutierrez *et al.*, our result agrees even better. The other paper[16] reported the effective thermal diffusivity (α_{eff}) for seven samples of n-type PSi with anodization times from 10 to 83 min without making relation to porosity. Their values range from 0.44 to 0.05 cm^2/s. For the same range of anodization time, our results go from 0.295 to 0.091 cm^2/s (see Table SM-II in the supplementary material), which gives an acceptable agreement between both results.

V. CONCLUSIONS

A methodology for determining the thermal properties of n-type porous silicon's porous layer as a function of its porosity was developed. The thermal diffusivity obtained from the porous layer of n-type porous silicon shows a constant value of around 0.076 cm^2/s independent of porosity. The analytical expressions deduced for the thermal conductivity, the volumetric heat capacity, and the thermal effusivity of the porous layer showed a decreasing linear dependence on the porosity as $k_{cp} = (1-p) \times 0.126$ W/cm K, $\rho_{cp}c_{cp} = (1-p) \times 1.66$ J/cm^3 K, and $e_{cp} = (1-p) \times 0.458$ W s$^{1/2}$/cm^{2}K. These results were obtained in the porosity values ranging from 0.279 to 0.702. The methodology reported here can help study the thermal properties of other porous materials with similar structures.

SUPPLEMENTARY MATERIAL

In the supplementary material, Table SM-I summarizes the measured values of the full sample thickness (l), porous layer thickness (l_1), porous layer thickness fraction ($x = l_1/l$), and the porosity (p) of each porous silicon sample, as well as the anodizing time of each sample's elaboration process. Table SM-2 shows the characteristic frequency of each PSi sample, obtained by best fitting Eq. (20) to the experimental data of photoacoustic measurements and their effective thermal diffusivity calculated from the characteristic frequency and the sample thickness using Eq. (21). The porosity value measured in each sample is also shown.

ACKNOWLEDGMENTS

The authors thank Consejo Nacional de Humanidades, Ciencia y Tecnología (CONAHCyT) and Secretaría de Investigación y Posgrado (SIP) from Instituto Politécnico Nacional (IPN), both of Mexico for supporting this work through research grants, scholarships to students, and incentives to researchers. The support from COFAA-IPN through the SIBE and BEIFI Programs of Mexico is also acknowledged. A. Rojas thanks the CONAHCYT support through Posdoctoral Fellowship Contract No. I1200/320/2022.

AUTHOR DECLARATIONS

Conflict of Interest

The authors have no conflicts to disclose.

Author Contributions

Joel Hernández-Wong, Uriel Nogal Luis, and Alejandro Rojas Marroquin contributed equally to this paper.

Joel Hernández-Wong: Investigation (equal); Resources (lead); Software (lead); Writing – review & editing (equal). **Uriel Nogal Luis:** Formal analysis (equal); Investigation (equal); Validation (lead); Writing – review & editing (equal). **Alejandro Rojas Marroquin:** Formal analysis (equal); Investigation (equal); Writing – original draft (equal). **Lizbeth Luviano Elizalde:** Data curation (lead); Investigation (equal); Writing – review & editing (equal). **José Bruno Rojas-Trigos:** Data curation (lead); Formal analysis (equal); Investigation (equal); Writing – review & editing (equal). **Ernesto Marin Moares:** Formal analysis (equal); Investigation (equal); Visualization (lead); Writing – review & editing (equal). **Antonio Calderon:** Conceptualization (lead); Formal analysis (equal); Funding acquisition (lead); Investigation (equal); Methodology (lead); Writing – original draft (lead); Writing – review & editing (equal).

DATA AVAILABILITY

The data that support the findings of this study are available from the corresponding author upon reasonable request.

REFERENCES

[1] L. Canham, "Routes of formation for porous silicon," in *Handbook of Porous Silicon*, edited by L. Canham (Springer International Publishing AG, part of Springer Nature, 2018).
[2] O. Kuntyi, G. Zozulya, and M. Shepida, Adv. Mater. Sci. Eng. **2022**, 1482877 (2022).
[3] F. Ronkel, J. W. Schultze. J. Porous Mater. **7**, 11–16 (2000).
[4] A. Loni, "Porous silicon formation by anodization," in *Handbook of Porous Silicon*, edited by L. Canham (Springer International Publishing AG, part of Springer Nature, 2018).
[5] F. Karbassian, "Porous silicon," in *Porosity—Process, Technologies and Applications*, edited by T. H. Ghrib (Intechopen, 2018).
[6] G. Amsel, E. d´Artemare, G. Battistig, V. Morazzani, and C. Ortega, Nucl. Instrum. Methods Phys. Res., Sect. B **122**, 99–112 (1997).
[7] A. Uhlir, Bell Syst. Tech. J. **35**, 333–347 (1956).
[8] L. Canham, "Chapter V. Applications," in *Handbook of Porous Silicon* (Springer International Publishing AG, part of Springer Nature, 2018).

[9]T. Tieu, M. Alba, R. Elnathan, A. Cifuentes-Rius, and N. Voelcker, Adv. Ther. **2**, 1800095 (2019).
[10]P. P. Sharma, S. Erfantalab, J. Dell, G. Parish, and A. Keating, Appl. Mater. Today **39**, 102320 (2024).
[11]Z. Cheng, H. Jiang, X. Zhang, F. Cheng, M. Wu, and H. Zhang, Adv. Funct. Mater. **33**, 2301109 (2023).
[12]N. Koshida, "Thermal properties of porous silicon," in *Handbook of Porous Silicon*, edited by L. Canham (Springer International Publishing AG, part of Springer Nature, 2018).
[13]K. Behzad, W. M. Mat Yunus, Z. Abidin Talib, A. Zakaria, A. Bahrami, and E. Shahriari, Adv. Opt. Technol. **2012**, 1 (2012).
[14]R. Srinivasan, M. Jayachandran, and K. Ramachandran, Cryst. Res. Technol. **42**, 266–274 (2007).
[15]S. Lettieri, U. Bernini, E. Massera, and P. Maddalena, Phys. Status Solidi C **2**, 3414–3418 (2005).
[16]A. Calderón, J. J. Alvarado-Gil, Y. G. Gurevich, A. Cruz-Orea, I. Delgadillo, H. Vargas, and L. C. M. Miranda, Phys. Rev. Lett. **79**, 5022–5025 (1997).
[17]J. J. Yon, K. Barla, R. Herino, and G. Bomchil, J. Appl. Phys. **62**, 1042–1048 (1987).
[18]Y. S. Touloukian, "Specific heat nonmetallic solids," in *Thermophysical Properties of Matter. The TPRC Data Series* (IFI/Plenum Data Corporation, New York, 1970), Vol. 5.
[19]Y. S. Touloukian, "Specific heat nonmetallic liquids and gases," in *Thermophysical Properties of Matter. The TPRC Data Series* (IFI/Plenum Data Corporation, New York, 1970), Vol. 6.
[20]Y. S. Touloukian, "Thermal conductivity nonmetallic liquids and gases," in *Thermophysical Properties of Matter. The TPRC Data Series* (IFI/Plenum Data Corporation, New York, 1970), Vol. 3.
[21]E. Martin, G. Ori, T. Q. Duong, M. Boero, and C. Massobrio, J. Non-Cryst. Solids **581**, 121434 (2022).
[22]Y. A. Cengel and A. J. Ghajar, *Heat and Mass Transfer Fundamentals & Applications*, 5th ed. (McGraw-Hill Companies, 2014).
[23]A. M. Mansanares, A. C. Bento, H. Vargas, N. F. Leite, and L. C. M. Miranda, Phys. Rev. B **42**, 4477 (1990).
[24]C. Vázquez-López, A. Calderón, M. E. Rodríguez, E. Velasco, S. Cano, R. Colás, and S. Valtierra, J. Mater. Res. **15**, 85–91 (2000).
[25]A. Calderón, R. A. Muñoz Hernández, S. A. Tomás, A. Cruz-Orea, and F. Sánchez Sinencio, J. Appl. Phys. **84**, 6327–6329 (1998).
[26]A. Wolf and R. Brendel, Thin Solid Films **513**, 385–390 (2006).
[27]A. Bruska, E. V. Astrova, U. Falke, T. Raschke, C. Radehaus, and M. Hietschold, Thin Solid Films **297**, 79–83 (1997).
[28]A. Gutiérrez, J. Giraldo, and M. E. Rodríguez-García, Rev. Mex. Fis. **57**(2), 99–105 (2011).
[29]A. Rosencwaig and A. Gersho, J. Appl. Phys. **47**, 64–69 (1976).

Supplementary Material

Table SM-I. Thicknesses and porous layer porosities of the PSi samples

Anodization time t_a (min)	Full sample thickness l (μm)	Porous layer thickness l_l (μm)	Porous layer thickness fraction $x = l_1 / l$	Porosity p
10	498 ± 15	87 ± 2	0.175 ± 0.009	0.279 ± 0.023
20	493 ± 15	134 ± 4	0.272 ± 0.016	0.351 ± 0.038
30	495 ± 15	172 ± 5	0.347 ± 0.021	0.414 ± 0.021
40	472 ± 14	188 ± 5	0.398 ± 0.022	0.479 ± 0.037
50	497 ± 15	214 ± 6	0.431 ± 0.025	0.558 ± 0.047
60	498 ± 15	238 ± 7	0.478 ± 0.028	0.590 ± 0.041
70	493 ± 14	249 ± 7	0.505 ± 0.029	0.619 ± 0.052
80	494 ± 15	266 ± 8	0.538 ± 0.033	0.647 ± 0.038
90	497 ± 15	282 ± 9	0.567 ± 0.035	0.674 ± 0.041
100	498 ± 15	296 ± 10	0.594 ± 0.038	0.702 ± 0.043

Table SM-II. Characteristic frequency, and effective thermal diffusivity of the PSi samples

Porosity p	Characteristic frequency f_c (Hz)	Effective thermal diffusivity α_{eff} (cm^2/s)
0.279 ± 0.023	37.6 ± 2.2	0.295 ± 0.030
0.351 ± 0.038	27.4 ± 1.9	0.215 ± 0.027
0.414 ± 0.021	18.7 ± 1.2	0.147 ± 0.018
0.479 ± 0.037	14.6 ± 0.9	0.115 ± 0.012
0.558 ± 0.047	15.3 ± 0.8	0.120 ± 0.013
0.590 ± 0.041	13.1 ± 0.6	0.103 ± 0.011
0.619 ± 0.052	12.8 ± 0.05	0.100 ± 0.005
0.647 ± 0.038	11.6 ± 0.05	0.091 ± 0.005
0.674 ± 0.041	11.3 ± 0.4	0.089 ± 0.004
0.702 ± 0.043	11.1 ± 0.3	0.087 ± 0.003